JOURNAL OF Materials CHEMISTRY

Synthesis, structure, and solid-state electrochemical properties of Cr_3BO_6: a new chromium(III) borate with the norbergite structure

J. L. C. Rowsell and L. F. Nazar

Department of Chemistry, University of Waterloo, Waterloo, Ontario, Canada N2L 3G1

Received 19th January 2001, Accepted 26th June 2001
First published as an Advance Article on the web 13th September 2001

A new compound in the Cr–B–O system with the $M^{III}_3BO_6$ norbergite structure has been synthesized by a solid state reaction. Rietveld refinement of the powder X-ray diffraction pattern in the space group *Pnma* yielded unit cell parameters of $a=9.8552(2)$, $b=8.4007(2)$, $c=4.4138(1)$ Å. The compound is formed in highest purity using a hydrated chromium(III) sulfate precursor, which has the highest decomposition temperature of the reagents used in this synthesis. A reaction scheme is proposed to explain this observation. The electrochemical properties of this material as a negative electrode for lithium-ion batteries were investigated and found to be similar to those for the previously studied Fe_3BO_6, although the average Li-uptake potential was lowered to 1.0 V.

Introduction

Metal borates exhibit a wealth of structural diversity, resulting in a broad range of electronic, magnetic, and optical properties. They hold promise for uses as zeolites,[1] in non-linear optical devices,[2] and as solid electrode materials.[3] Their variation in structure arises from the ability of boron to be either three- or four-coordinated by oxygen in the lattice; often forming metaborates that have extended networks surrounding metal oxide polyhedra. These differ from orthoborates, where discrete borate trigonal planes or tetrahedra are imbedded in a metal oxide framework.[4] Transition metal orthoborates fall into roughly five structural classes: those with the calcite structure $M^{III}BO_3$,[5,6] the kotoite structure $M^{II}_3(BO_3)_2$,[7] the oxyborates (including warwickite, ludwigite, and related forms),[8] the zircon structure $M^{V}BO_4$,[9] and the norbergite structure $M^{III}_3(BO_4)O_2$.[10] Of these, the latter contain only tetrahedral BO_4 groups, a characteristic that appears to be rare, and true for the metaborate, $M^{II}_4(BO_3)_6O$.[11,12]

The utility of borates and other oxides as electrode materials for lithium-ion batteries received an upswing in interest recently, following the publication in *Science* in 1997 of a tin aluminophosphoborate glass as a negative electrode for the low potential uptake of Li ions.[13] Currently graphitic carbon is used in commercial Li-ion cells,[14] although its modest reversible gravimetric capacity of <370 mA h g^{-1} and low volumetric capacity are thought to be limiting for future technologies. Materials such as transition metal oxides and/or orthoborates that exhibit low-potential insertion properties present a possible advantage. A variety of metal oxides,[15] tin borate glasses,[16] and metal borates[3,17] have been examined intensely for their Li cycling properties. Transition metal orthoborates should exhibit better properties than metaborates for this purpose, as they have a higher metal content resulting in a larger theoretical capacity. The norbergite structure has the second highest metal content per formula unit (behind ludwigite, ideally $M^{III}M^{II}_2(BO_3)O_2$), and, thus far, our electrochemical studies on low-potential Li uptake properties have focussed on this material. Until now, the structure was only established for M^{III} = Fe or Al, the latter requiring a high pressure solid state synthesis.[18] Our preliminary results for the uptake of Li by Fe_3BO_6 showed interesting behavior, with a reversible specific capacity of 450 mA h g^{-1}.[3] These studies led us to search for new members of the norbergite family.

The oxide chemistry of chromium has been primarily studied for catalytic applications, which have been known for some time.[19] The decomposition of its salts, hydroxides, and hydrous oxides to Cr_2O_3 all appear complete below 600 °C in air.[20–22] Only one chromium borate has been reported so far: $CrBO_3$.[23] By careful choice of starting materials, we have synthesized the new compound Cr_3BO_6, demonstrating yet another parallel between chromium and iron chemistry. Several differences exist between these two M^{III}–B–O systems, however, and these have been studied by a combination of powder X-ray diffraction (XRD), thermogravimetric and differential thermal analysis (TGA–DTA), and scanning electron microscopy (SEM). These observations have then been applied to explain the similar electrochemical behaviour of the two norbergite materials.

Experimental

Synthesis

Optimum preparation of the title compound was achieved with a finely ground mixture of $Cr_2(SO_4)_3{\cdot}xH_2O$ (Aldrich, $x\sim6$) and H_3BO_3 (Baker, 99.8%) in a 1 : 4 molar ratio. The mixture was ground in a planetary ball mill (Fritsch) for a total of 30 min using a sialon-composite grinding set. The fine green powder was then pressed into pellets 12.5 mm in diameter and ~5 mm in thickness under a pressure of 10 metric tons and fired in alumina boats (Alfa Aesar) for three days at 680 °C after ramping to this temperature by 5 °C min^{-1}. After quenching in air, the dark grey–green pellets were ground and washed with water to remove the unreacted boron oxide. Rietveld refinement of the powder XRD pattern (see below) revealed the product contained $\sim11\%$ Cr_2O_3 impurity.

Additional firings were performed with Cr_2O_3 (Aldrich, 98%), $Cr(NO_3)_3{\cdot}9H_2O$ (Baker, 99%), or freshly precipitated $Cr(OH)_3{\cdot}3H_2O$ as the chromium source. The hydrated chromium hydroxide was prepared by adding 2 M NH_3 (aq) to a rapidly stirred solution of 0.5 M $Cr(NO_3)_3{\cdot}9H_2O$ to pH ~10. The suspension was filtered through a glass frit, washed with water, and dried overnight in the filter crucible under suction. The purity of this reagent was confirmed by TGA, as described below. Mixtures of these reagents with boric

 DOI: 10.1039/b100707f

acid were prepared for various Cr : B ratios between 3 : 1 and 1 : 8 and fired at various temperatures in the range 600–1000 °C, each for three days.

Structure determination

The structural similarity between the title compound and Fe_3BO_6 was immediately evident from a comparison of their powder diffraction patterns. The unit cell parameters and peak profile coefficients were first determined by the Le Bail method using the GSAS refinement program.[24] Reflections due to the Cr_2O_3 impurity were used as an internal standard.[25] Rietveld refinement was initiated using the atomic coordinates of Fe_3BO_6[26] and converged with the final agreement values of $R_p = 0.0768$, $R_{wp} = 0.1102$. No correction was made for absorption or extinction.

Instrumental

Powder X-ray diffraction patterns of samples were collected in Bragg–Brentano geometry using a Siemens D500 diffractometer equipped with a diffracted beam monochromator (Cu-Kα radiation). Thermogravimetric analysis was performed with a PL Thermal Sciences STA 1500 apparatus, typically heating a 10 mg sample to 1000 °C at 10 °C min^{-1} under a 15 mL min^{-1} air flow. A LEO FE-SEM 1530 microscope operated at 15 kV was used to obtain images of the product.

The lithium storage capacity of the title material at low potential was investigated by electrochemically cycling a Cr_3BO_6 electrode contained in a Swagelok™ cell, with a metallic lithium counter-electrode serving as the Li-ion source and 1 M $LiPF_6$ in ethylene carbonate (EC)–dimethyl carbonate (DMC) (Merck) as the electrolyte. Electrodes were prepared as previously reported with 70% active material, 24% acetylene black to enhance electronic conduction, and 6% poly(vinylidene fluoride) (Aldrich) as a binder; mixtures (typically 5 mg of active material) were cast on nickel discs (1.13 cm^2) as cyclopentanone slurries. Galvanostatic cycling was performed using a MacPile system at a cycling rate of 1 Li/10 h, corresponding to a current density of 10 mA g^{-1} (51 μA cm^{-2}).

Results and discussion

Synthesis

The only known chromium borate to date is the calcite phase $CrBO_3$, formed from a melt of the oxide precursors[23] or as the side product of a gas phase transport reaction.[6] In both cases the reaction temperature was above 900 °C, and the product was found to be stable to 1220 °C. In this region volatilization of boron oxide becomes a problem, and this is perhaps why a phase diagram for this system has not been reported. The phase diagram of the Fe_2O_3–B_2O_3 system has been proposed, where it was shown that the iron-containing phase in the B_2O_3-rich region is independent of stoichiometry.[27] In an excess of boron oxide, the reaction pathway appears to be that shown in Scheme 1. All of our attempts to mimic this reaction scheme with Cr_2O_3 failed, the only products being $CrBO_3$ and/or Cr_2O_3. Other aailable sources of chromium(III) were therefore employed.

We found we could obtain crystalline Cr_3BO_6 by using hydrated chromium(III) salts, at even lower temperatures than expected. In the presence of boric acid, mixtures of poorly crystalline product and Cr_2O_3 were observed when using $Cr(OH)_3{\cdot}3H_2O$ as the chromium source, for Cr : B ratios between 2 : 1 and 1 : 2 heated in the temperature range 660–720 °C. The low degree of crystallinity of the product was apparent from broadening of the XRD reflections. As higher purity could be achieved by using alternate reagents, further studies with this precursor were not performed. Decomposition of the nitrate salt yielded 80% pure Cr_3BO_6 for Cr : B = 1 : 2

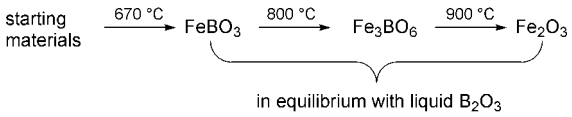

Scheme 2

after firing the mixtures for three days at 680 °C, following an initial heating step at 300 °C for 16 h, and regrinding. The purity of the washed sample was determined by Rietveld refinement. The title compound forms as the major phase between 650 and 720 °C for compositions between 1 : 1 and 1 : 3 (Cr : B). Below this temperature, the products are poorly crystalline, while above 720 °C the proportion of Cr_2O_3 increases. At both higher and lower Cr compositions, Cr_2O_3 is the main phase; and Cr_3BO_6 is not observed at all for Cr : B < 1 : 4.

Better results were obtained with the sulfate salt, where Cr_3BO_6 was formed in a wider compositional range—between 3 : 1 and 1 : 4 (Cr : B)—and in higher purity. The thermal evolution of the 1 : 2 mixture is illustrated in Fig. 1. For temperatures below 660 °C, unreacted $Cr_2(SO_4)_3$ is evident in the X-ray pattern; the same is true for compositions < 1 : 4. Product purities approaching 90% were obtained using this reagent by pressing the reaction mixture into pellets prior to firing. The integrity of the pellets was maintained during calcination, indicating slow outgassing during decomposition. Regrinding and annealing of the mixture did not improve sample purity, nor did the use of shorter firing times. The latter resulted in incomplete reaction: for a 1 : 2 mixture fired for 14 h, only a small amount of Cr_3BO_6 was formed. In the case of the 1 : 2 nitrate mixture, firing for 14 h gave a poorly crystallized product of the same 80% purity as the product obtained in three days.

In summary, thermal decomposition of hydrated chromium(III) salt precursors, particularly the sulfate salt, allowed for the nearly pure synthesis of Cr_3BO_6 in a compositional range smaller than that of the analogous iron(III) borate phase. It is noteworthy that each of the precursors yields the title phase only in B_2O_3-rich mixtures, as observed for the formation of Fe_3BO_6.[27] Clearly boron oxide is necessary as both a reagent and a flux to facilitate crystal growth.

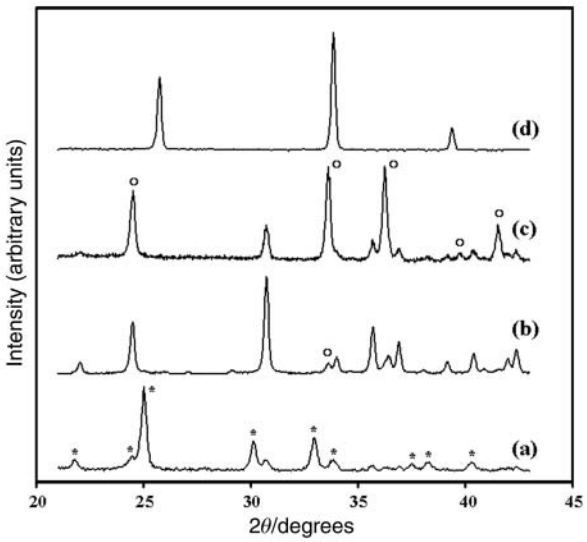

Fig. 1 Powder XRD patterns of a $Cr_2(SO_4)_3{\cdot}xH_2O + 4\ H_3BO_3$ mixture pressed and fired at (a) 14 h at 680 °C, (b) 3 days at 680 °C, (c) 1 day at 800 °C, (d) 3 days at 900 °C. Samples (b)–(d) were washed to remove B_2O_3. The impurities $Cr_2(SO_4)_3$ and Cr_2O_3 are indicated by asterisks and open circles, respectively. The pattern in (b) is 89% pure Cr_3BO_6, with only the (100) reflection of Cr_2O_3 clearly resolved. The pattern in (d) is that of pure $CrBO_3$.

Reagent thermal stability

Previous thermogravimetric analyses show that Cr_2O_3 is formed at 400 °C from $Cr(NO_3)_3{\cdot}9H_2O$,[20] 470 °C from $Cr(OH)_3{\cdot}3H_2O$,[21] and 560 °C (*in vacuo*) from $Cr_2(SO_4)_3$.[22] The principle weight loss steps for the first two compounds occur below 300 °C, resulting in a black, poorly crystalline material consisting of CrO_2 and/or CrOOH. The interconversion between these two intermediates has been studied recently.[28] For the sulfate hydrates, dehydration is complete at 500 °C to form the crystalline anhydrous salt.[29] Our TGA–DTA analyses show agreement with these results—and some discrepancies. For the hydroxide, we found that the final weight loss step occurs at 410 °C, under either air or dry nitrogen, with a weight loss of 5% as shown in Fig. 2(a). This evidently corresponds to the transformation of CrOOH and/or CrO_2 to Cr_2O_3, and not the loss of chemisorbed gases as previously suggested,[21] providing better consistency with the decomposition processes occurring in the nitrate salt. It should be noted that there is virtually no difference between these results and those obtained by ramping up the temperature at 2 °C min^{-1}. The total weight loss of this sample was 50%, indicating some of the sample was dehydrated during the drying procedure, to give a starting composition closer to $Cr(OH)_3{\cdot}2.7H_2O$. This is expected to have little or no impact on the observations of the bulk decomposition temperature or the behaviour of the reagent during calcination.

More important to this synthesis is the decomposition of the hydrated sulfate salt in air. As shown in Fig. 2(b), the $Cr_2(SO_4)_3{\cdot}xH_2O$ proceeds through a slow dehydration commencing at ~120 °C, followed by a sharp loss of water at 400 °C, and finally a gradual volatilization of SO_3 centered at 675 °C. The weight losses for each step are 16, 6, and 48%, corresponding to the respective loss of 4.5 molecules of H_2O, 1.5 H_2O and 3 SO_3 per formula unit (leading to the conclusion that $x=6$ in the reagent formula). Powder XRD experiments show that the product transforms through a series of amorphous and crystalline phases on heat treatment; from amorphous below 400 °C, to the crystalline anhydrous salt at 500 °C, to amorphous at 680 °C, and finally to crystalline Cr_2O_3 at 800 °C. These observations are in qualitative agreement with the literature.[22,29] When the TGA–DTA ramp rate is decreased to 2 °C min^{-1} (as used in ref. 22), the temperatures of the decomposition events are lowered to 375 and 620 °C, respectively. The discrepancy between our decomposition temperature and the previously reported value is, therefore, solely due to the difference in atmosphere; namely the previous analysis was conducted at low pressure instead of under a gas flow. The observation of an amorphous oxygen-rich phase prior to Cr_2O_3 crystallization also implies the presence of CrO_2 as an intermediate species.

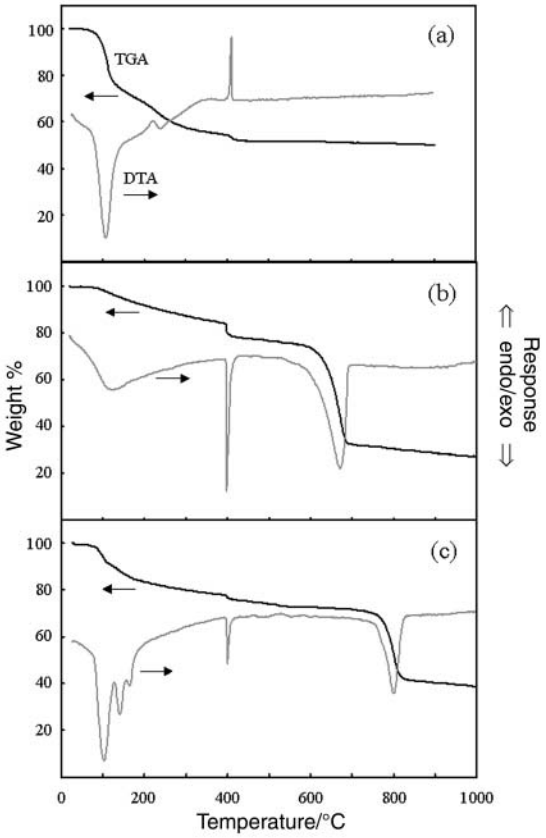

Fig. 2 TGA–DTA curves of (a) $Cr(OH)_3{\cdot}xH_2O$ ($x\sim2.7$), (b) $Cr_2(SO_4)_3{\cdot}xH_2O$ ($x\sim6$), and (c) a $Cr_2(SO_4)_3{\cdot}xH_2O+4\ H_3BO_3$ mixture.

Reaction mechanism

Thermal analysis was also employed in an attempt to elucidate the phase boundaries of this system. Although this was precluded by the extremely slow kinetics of the borate phase transitions, important information was nonetheless gleaned from the results. Thermograms of Cr_3BO_6 and $CrBO_3$ revealed no distinguishable endo- or exotherms and only minimal weight loss. Examination of powder XRD patterns at various stages of heat treatment showed that Cr_3BO_6 is stable at 800 °C for one day, but converts almost completely to Cr_2O_3 and $CrBO_3$ in three days. An unwashed sample of the product (Cr : B = 1 : 2), however, only decomposes to a small degree after three days. The stabilizing effect of the boron oxide matrix is also exhibited in the TGA–DTA of the starting materials. In Fig. 2(c), when the sulfate precursor is mixed with boric acid, the final decomposition point is shifted to 800 °C (the additional dehydration steps below 200 °C are due to H_3BO_3). This is consistent with our observation that complete reaction requires about three days at 680 °C. The XRD pattern of the material after TGA analysis shows only faint reflections of Cr_3BO_6 amidst the intense lines of Cr_2O_3.

These results allowed us to correlate the success of each reagent in forming the target compound. For mixtures with boron oxide, the formation of Cr_3BO_6 appears to compete with the formation of Cr_2O_3 in the temperature range 650–720 °C. In each case, an amorphous intermediate is formed, probably CrO_x ($1.5<x<2$) stabilized in the boron oxide matrix. Assuming that the crystal growth rates of both products are roughly similar, the competition is actually between the number of incipient nucleation sites. If the intermediate is formed slowly, as is the case for the sulfate mixture, then these oxides will diffuse into the boron oxide and nucleate formation of the borate. If it is formed too quickly, then oxidic aggregates form, nucleating Cr_2O_3. This proposed reaction scheme is illustrated in Scheme 2. Assuming all unimolecular reactions, the rates can be compared by their rate constants, k_i. If k_1 is large, as is the case for all reagents above 800 °C, then $k_2<k_3$ and Cr_2O_3 is the main product. If k_1 is small, as is the case for the sulfate mixture at 680 °C, then $k_2>k_3$ and more Cr_3BO_6 is formed.

Finally, the phase transitions in this binary system can be compared to those of the analogous iron system. In the boron rich region between Cr : B = 1 : 1 and 1 : 4, the simplified

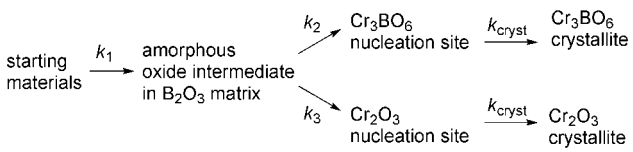

Scheme 2 Proposed reaction scheme for the decomposition of chromium(III) salts in boron oxide. The rate of decomposition k_1 ultimately determines the nucleation rates of Cr_3BO_6 and Cr_2O_3, which then controls the sample purity, assuming similar rates of crystal growth.

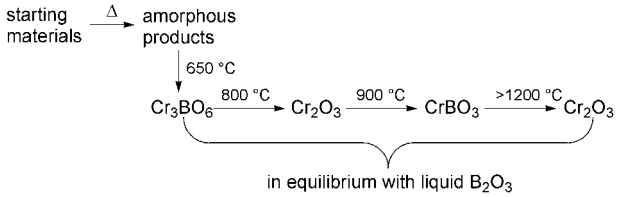

Scheme 3

pathway that is followed by hydrated salt precursors is summarized in Scheme 3. In this pathway, Cr_2O_3 is assumed to be the necessary precursor to $CrBO_3$. This reaction pathway follows a different order than outlined for Fe_3BO_6 (*vide supra*).

Structure

The powder XRD pattern of Cr_3BO_6 is shown in Fig. 3, along with the fitted profile refined by the Rietveld method. It is similar to the pattern calculated from single crystal data of Fe_3BO_6,[26] with additional peaks ascribed to Cr_2O_3. By fixing the parameters for the Cr_2O_3 phase during refinement, the structural data listed in Tables 1 and 2 for Cr_3BO_6 were obtained. The final phase fractions were 88.6% Cr_3BO_6 and 11.4% Cr_2O_3. Selected bond lengths and angles are shown in Fig. 4(a) and (c), illustrating the coordination environments of chromium and boron in the structure. The oxygen atoms form a distorted hexagonal close-packed lattice that forms layers perpendicular to [001], with two crystallographically independent Cr^{3+} ions filling one-half of the octahedral sites. These are edge-shared in layers parallel to (001), forming 3×3 "zig-zags" running along [010]. One twelfth of the tetrahedra are occupied by boron, and share corners that connect the layers. Occupation of any of the remaining sites leads to the unfavourable situation of tetrahedral face-sharing, implying structural instability on Li^+ insertion, as shown in our studies of Fe_3BO_6. Further details concerning the parent norbergite structure and its relation to olivine have been previously described.[3,30]

More interesting are the differences in coordination sites between the iron and chromium structures. As illustrated in Fig. 4, the bond lengths and angles show a more regular octahedral environment for chromium, paralleling the corundum structures of Cr_2O_3 and Fe_2O_3.[31] In contrast, the BO_4 tetrahedron is elongated in Cr_3BO_6, compared to the less distorted tetrahedron observed in Fe_3BO_6. Perhaps distortion of this tetrahedral site (towards a trigonal environment) makes

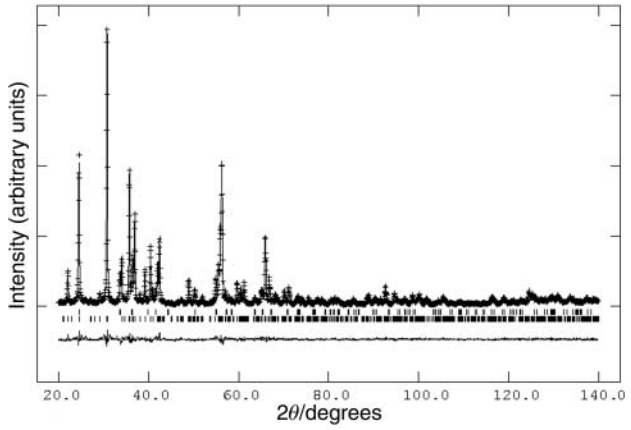

Fig. 3 Powder XRD pattern of Cr_3BO_6 with 11.4% Cr_2O_3 impurity. Observed data are indicated by (+) marks; the calculated pattern and difference curves are shown by solid lines. The first row of tick marks below the observed data indicates the positions of Cr_2O_3 reflections and the second row of tick marks are the calculated Cr_3BO_6 reflections positions.

Table 1 Crystallographic data for Cr_3BO_6

Empirical formula	BCr_3O_6
Formula weight	262.80
Sample form	Dark grey/green powder
Crystal system	Orthorhombic
Space group	*Pnma*
Unit cell dimensions/Å	$a = 9.8552(2)$
	$b = 8.4007(2)$
	$c = 4.4138(1)$
Volume/Å^3	365.42(2)
Z	4
Calculated density/g cm^{-3}	4.777
Secondary phase (fraction)	Cr_2O_3 (0.114)
Wavelength/Å	1.54178
Refinement Method	Rietveld, using GSAS software
Extinction/absorption correction	Not applied
Data range/°	$20 < 2\theta < 140°$
Parameters	42
R_p	0.0768
R_{wp}	0.1102

Table 2 Atomic coordinates and isotropic temperature factors for Cr_3BO_6

Atom	Wyckoff site	x	y	z	U_{iso}/Å^2
Cr1	8d	0.1279(1)	0.0685(1)	0.9928(5)	0.003(1)
Cr2	4c	0.4043(2)	0.2500(0)	0.9796(7)	0.003(1)
B1	4c	0.219(1)	0.2500(0)	0.425(3)	0.010(5)
O1	8d	0.2887(6)	0.1067(7)	0.2656(10)	0.004(2)
O2	8d	0.4660(6)	0.0833(7)	0.7362(9)	0.003(2)
O3	4c	0.0792(8)	0.2500(0)	0.2795(14)	0.003(2)
O4	4c	0.2238(9)	0.2500(0)	0.7555(14)	0.009(3)

it the "weak link" of the structure, lowering the thermal stability of the chromium(III) borate. This may be explained by the trend in ionic radii, where a larger metal ion at the octahedral site favours a more regular BO_4 unit and thus stabilizes the norbergite phase over the calcite phase (which contains only trigonal BO_3 units). Therefore the predicted trend in stability of the norbergite would be $Fe^{3+} > Cr^{3+} > Al^{3+}$, based on ionic radii.[32] High pressures would be required for smaller ions, and effectively "force" a fourth oxygen into boron's coordination sphere. These arguments are in accord with the observed results: note that Al_3BO_6 is only formed at very high pressure, whereas the calcite phase is observed at lesser pressures. Furthermore, the $Hg_4(BO_3)_6O$ and the M^VBO_4 phases, which also contain only BO_4 tetrahedra, are formed only under high pressure conditions.[9,12]

Particle size determination

In our electrochemical studies of Fe_3BO_6, a difference in the working voltage for the electrochemical curves on discharge and charge was observed. Such hysteresis or polarization is common to all materials under fast cycling rates but is especially prominent where phase changes occur on Li-(de)insertion, and/or where kinetic impediments are present. In the case of the iron(III) borate, as here, hysteresis in the cycling curves is related to the firing temperature and consequent particle size of the material. Nanoparticulate iron(III) borate showed a greater initial specific capacity than for micron-sized particles prepared at higher temperatures, but this faded rapidly on cycling and a larger polarization was observed.

Line broadening in the XRD pattern of Cr_3BO_6 (that is not observed in micron-sized Fe_3BO_6) suggests that the coherence length in the particles is relatively short, as a result of defects or a very small particle size. This could be a consequence of the low synthesis temperature which is similar to that used for nanoparticulate iron(III) borate. SEM imaging of a typical sample of washed Cr_3BO_6, shown in Fig. 5, confirmed that the

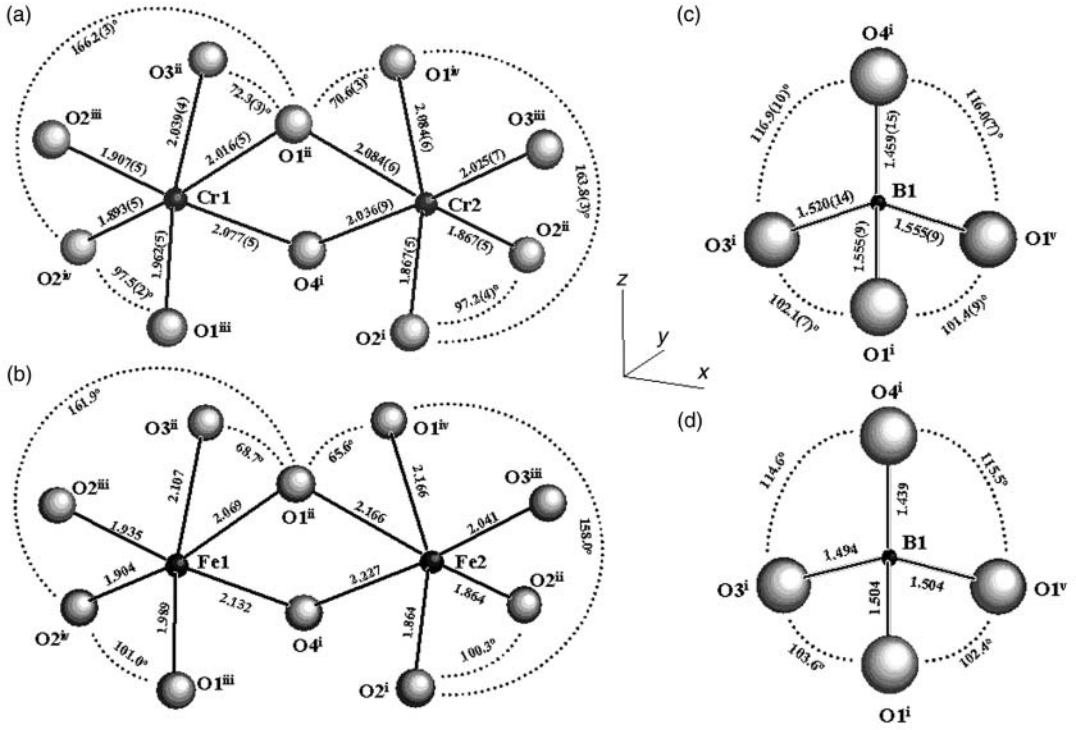

Fig. 4 The two crystallographically independent metal octahedra for (a) M = Cr and (b) M = Fe and the boron tetrahedra for (c) M = Cr and (d) M = Fe in M_3BO_6. The labelling scheme is the same as that used in ref. 26. Selected bond lengths and angles in Cr_3BO_6 are shown with estimated standard deviations in parentheses. All bond angles shown are for O–X–O (X = M or B) with the oxygens situated at the ends of dotted arcs. The deviations from ideal octahedral coordination of M are more pronounced in Fe_3BO_6 (data from ref. 26), while the BO_4 tetrahedron is more distorted in Cr_3BO_6.

particle size is in the "nano"-regime. The particles are arranged in sub-micron sized aggregates of crystallites that are each $\sim$100 nm in size. We were unable to differentiate Cr_3BO_6 crystallites from Cr_2O_3, and it is probable that they are intergrown in these aggregates. Still, their tiny size and propensity for polycrystallinity supports the reaction scheme of Scheme 2, and the lack of distinct habits or abnormally large crystallites is in accord with the assumption that the crystal growth rates of the two phases are the same at this firing temperature.

Electrochemistry

Our electrochemical experiments were aimed at directly comparing the analogous chromium(III) and iron(III) borates. In Fig. 6, the first discharge–charge curve of Cr_3BO_6 has been overlaid with that previously reported for nanoparticulate Fe_3BO_6 formed at 700 °C (hereafter referred to as nano-Fe_3BO_6).[3] The general features of both curves are the same. For the chromium(III) borate, the first two processes are not characteristic of the material itself; namely the first uptake of 0.9 Li (process *a*) corresponds to insertion into carbon (the conductive additive), whereas the Cr_2O_3 impurity accounts for the following 0.4 Li at 0.7 V (process *b*). This was established by performing Li insertion experiments on these materials alone. Uptake of lithium in Cr_3BO_6 is characterized by a slightly sloping plateau at 0.35 V (process *c*) that signals the same decomposition process exhibited by Fe_3BO_6 at 1.4 V. Of the total of 9.9 Li taken up by the composite, 8.6 Li are therefore ascribed to the Cr_3BO_6 phase, suggesting that nearly full reduction of the chromium is achieved on discharge ($3Cr^{3+} + 9e^- \rightarrow 3Cr^0$). *Ex situ* powder XRD analysis (under argon, within a sealed sample holder) confirmed the material was amorphous after reduction.

Importantly, this process is partially reversible on oxidation. The product at the end of charge remains amorphous and thus

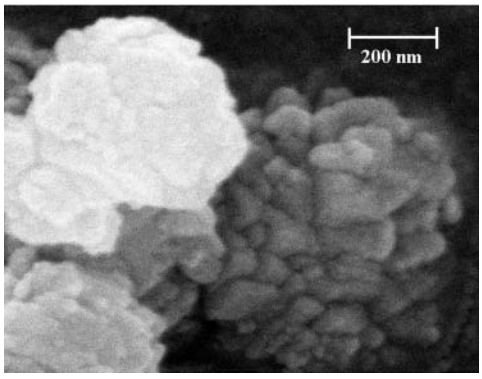

Fig. 5 Scanning electron microscope image of Cr_3BO_6 aggregates less than 1 μm in size that are formed from crystallites 100–200 nm in size.

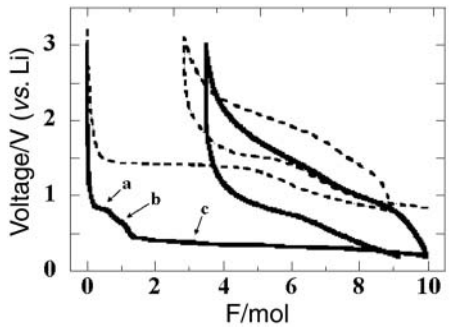

Fig. 6 The discharge–charge curves of Cr_3BO_6 in the voltage window 0.2–3.0 V (solid line) and Fe_3BO_6 in the voltage window 0.8–3.1 V (dotted line) cycled at 1 Li/10 h (current density of 10 mA g^{-1}). The different voltage windows chosen for the two materials reflect their differences in hysteresis and average Li-uptake potential. The small kinks indicated in the solid curve are due to Li uptake by (a) acetylene black and (b) Cr_2O_3. The plateau (c) at 0.35 V is the result of Li uptake by the title compound.

the exact nature of the oxidation process cannot be easily determined. As in the case of the iron borate and other metal–oxide systems, however, it probably results in consumption of the metal particles and re-formation of metal–oxygen bonds.[3,15] The reversible specific capacity for the first oxidation (690 mA h g^{-1}) is very similar to the capacity (700 mA h g^{-1}) achievable for nanoparticulate iron(III) borate. Unfortunately, as in the nano-Fe_3BO_6, polarization and fading of the initial capacity on cycling is also observed: only 280 mA h g^{-1} is maintained after 10 cycles. Since the chromium(III) borate was prepared within the same temperature regime, and washed using the same procedure as nano-Fe_3BO_6, it is probable that its surface properties are also similar. As shown above, the small particle size of Cr_3BO_6 is similar to nano-Fe_3BO_6, strongly suggesting that a high surface area and/or large number of surface-active groups are detrimental to the electrochemical performance. Adverse processes involving the solid–electrolyte interface may also cause the exaggerated hysteresis.

Although the electrochemical properties of Cr_3BO_6 that have been discussed so far are admittedly less than ideal, one success was achieved: the lowering of the average Li-uptake potential in this structure. The average uptake potential for nano-Fe_3BO_6 is 1.7 V (Fig. 6), while for Cr_3BO_6 it is 1.0 V. This is expected based on the aqueous reduction potentials of the two trivalent cations, and puts Cr_3BO_6 more firmly in the anode realm of application. It would be a possibly viable material if the cycling behavior and polarization could be improved. One approach is to increase the particle size, as this was beneficial for the analogous iron compound. Micron-sized particles prepared at higher temperature exhibited a distinct improvement in their electrochemical properties with a reversible specific capacity of 450 mA h g^{-1} at an uptake potential of 1.6 V, with reduced hysteresis.[3] Such particle-growth experiments for Cr_3BO_6 are presently underway.

Conclusions

The new compound Cr_3BO_6 has been prepared in 89% pure form by solid state reaction between hydrated chromium(III) sulfate and boric acid. Crystallites $\sim$100 nm in size have been observed by SEM. The compound is isostructural with Fe_3BO_6, one of a rare number of transition metal borates containing only tetrahedrally-coordinated boron. Rietveld refinement of powder XRD data shows the structure has less distortion in the MO_6 octahedral sites, but greater distortion of the BO_4 tetrahedra compared to the iron(III) borate. The latter feature may be responsible for the low thermal stability of the material. The proposed reaction scheme for chromium(III) borates involves an amorphous oxidic intermediate for the formation of Cr_3BO_6, and follows a pathway nearly reverse to that of the iron system. The product purity has been correlated with the choice of starting materials, and TGA has shown that it increases with the decomposition temperature of the chromium(III) salt. For $Cr_2(SO_4)_3$, sulfur trioxide loss is shown to occur between 620 and 680 °C under flowing air.

Electrochemically, the material behaves more poorly than the previously studied iron(III) borate, showing capacity fading on cycling and a large polarization. This has been correlated with particle size and preparation temperature, although it is still unclear which is the more important variable. The redeeming quality of this compound is that it has an average Li-uptake potential $\sim$0.6 V lower than Fe_3BO_6, which is advantageous for a material used as a low-potential, negative electrode. One clear course of action is to grow larger crystallites; however, attempts at recrystallization from a flux have lead to side reactions of the compound. A high-pressure synthesis may be necessary, as is required for many other metal orthoborates containing tetrahedral BO_4 units, and it is entirely possible that each of the calcite-MBO_3 forming metals can form a norbergite phase under those conditions.

Acknowledgements

L. F. N. gratefully acknowledges funding from the NSERC operating grants program and J. R. thanks NSERC for an Undergraduate Research Award.

References

1 R. Millini, G. Perego and G. Bellussi, *Top. Catal.*, 1999, **9**, 13.
2 P. Becker, *Adv. Mater.*, 1998, **10**, 979.
3 J. L. C. Rowsell, J. Gaubicher and L. F. Nazar, *J. Power Sources*, 2001, **97–98**, 254.
4 A. F. Wells, *Structural Inorganic Chemistry*, Oxford University Press, Oxford, 5th. edn., 1984, p. 1065ff.
5 I. Bernal, C. W. Struck and J. G. White, *Acta Crystallogr.*, 1963, **16**, 849.
6 H. Schmid, *Acta Crystallogr.*, 1964, **17**, 1080.
7 S. V. Berger, *Acta Chem. Scand.*, 1949, **3**, 660; R. E. Newnham, R. P. Santoro, P. F. Seal and G. R. Stallings, *Phys. Status Solidi*, 1966, **16**, K17.
8 Y. Takeuchi, N. Haga, T. Kato and Y. Miura, *Can. Mineral.*, 1978, **16**, 475 and references therein.
9 K-J. Range, M. Wildenauer and A. M. Heyns, *Angew. Chem., Int. Ed. Engl.*, 1988, **27**, 969.
10 J. G. White, A. Miller and R. E. Nielsen, *Acta Crystallogr.*, 1965, **19**, 1060.
11 P. Smith, S. Garcia-Blanco and L. Rivoir, *Z. Kristallogr.*, 1961, **115**, 460.
12 C. H. Chang and J. L. Margrave, *Inorg. Chim. Acta*, 1967, **1**, 378.
13 Y. Idota, T. Kubota, A. Matsufuji, Y. Maekawa and T. Miyasaka, *Science*, 1997, **276**, 1395.
14 S. Flandrois and B. Simon, *Carbon*, 1999, **37**, 165.
15 C. Sigala, D. Guyomard, Y. Piffard and M. Tournoux, *C.R. Acad. Sci. Paris II*, 1995, **320**, 523; F. Leroux, G. R. Goward, W. P. Power and L. Nazar, *Electrochem. Solid State Lett.*, 1998, **1**, 255; P. Poizot, S. Laruelle, S. Grugeon, L. Dupont and J-M. Tarascon, *Nature*, 2000, **407**, 496.
16 I. A. Courtney and J. R. Dahn, *J. Electrochem. Soc.*, 1997, **144**, 2943.
17 V. Legagneur, Y. An, A. Mosbah, R. Portal, A. Le Gal La Salle, A. Verbaere, D. Guyomard and Y. Piffard, *Solid State Ionics*, 2001, **139**, 37.
18 J-J. Capponi, J. Chenavas and J-C. Joubert, *Bull. Soc. Fr. Mineral. Cristallogr.*, 1972, **95**, 412.
19 W. A. Lazier and J. V. Vaughen, *J. Am. Chem. Soc.*, 1932, **54**, 3080.
20 N. E. Fouad, H. Knozinger, M. I. Zaki and S. A. A. Mansour, *Z. Phys. Chem.*, 1991, **171**, 75.
21 L. Spiccia, W. Marty and R. Giovanoli, *Helv. Chim. Acta*, 1987, **70**, 1737.
22 A. Noel, J. Tudo and G. Tridot, *Bull. Soc. Chim. Fr.*, 1968, **1**, 91.
23 N. C. Tombs, W. J. Croft and H. C. Mattraw, *Inorg. Chem.*, 1963, **2**, 872.
24 A. C. Larson and R. B. Von Dreele, *General Structure Analysis System (GSAS)*, Los Alamos National Laboratory Report LAUR 86-748, Los Alamos, NM, 2000.
25 H. Sawada, *Mater. Res. Bull.*, 1994, **29**, 239.
26 R. Diehl and G. Brandt, *Acta Crystallogr., Sect. B*, 1975, **31**, 1662.
27 H. Makram, L. Touron and J. Loriers, *J. Cryst. Growth*, 1972, **13**(14), 585.
28 M. Maciejewski, K. Kohler, H. Schneider and A. Baiker, *J. Solid State Chem.*, 1995, **119**, 13.
29 G. Watelle-Marion and R. Thiard, *C. R.. Acad. Sci. Paris*, 1965, **261**, 4105.
30 W. H. Taylor and J. West, *Z. Kristallogr.*, 1929, **70**, 461.
31 C. T. Prewitt, R. D. Shannon, D. B. Rogers and A. W. Sleight, *Inorg. Chem.*, 1969, **8**, 1985.
32 R. D. Shannon, *Acta Crystallogr., Sect. A*, 1976, **32**, 751.